Axial Dispersion of Solid Particles in a Continuous Rotary Kiln

Tamar Kohav, James T. Richardson, and Dan Luss
Dept. of Chemical Engineering, University of Houston, Houston, TX 77204

Six algorithms following single particle trajectories are used to predict the axial dispersion in rolling or slumping flow in a continuous rotary kiln. Models incorporating different physical phenomena show that axial dispersion is affected by the Froude number, L/D ratio, solid fill level, and rolling or slumping layer thickness. The main cause of axial dispersion is segregation of the particles roll or slump distance, due to variation of the solid flow properties caused by nonuniform particle size, density and shape. In a rolling bed with uniform particles the rolling layer thickness and the time of roll have to be accounted for in the prediction of the dispersion. The Peclet numbers computed for solid particles with uniform physical properties are of the order of 10^4. The solid segregated motion may lead to Peclet numbers of the order of $10 - 10^3$, a much larger dispersion. The main obstacle for a-priori prediction of the axial dispersion is lack of a reliable relation between the segregated roll or slump distance and the variation in particles properties, as well as the change in segregation as the flow properties of particles are changed during calcination.

Introduction

Continuous rotating drums have been widely used in the chemical and metallurgical industries for a long time. Short smooth drums ($L/D \approx 2$–5) with end constrictions are used for mixing powders as well as for grinding granular materials. Medium length rotating drums ($L/D \approx 5$–20), equipped with flights, are used for drying or cooling solid materials. Long ($L/D \approx 40$) rotating kilns, which are often equipped with flights and constrictions, are used for high temperature calcination of granular or powdered solids. Examples of processes carried out in continuous rotary kilns (CRK) include: calcination of iron (Sass, 1969), phosphate ores (Mu and Hard, 1984), and limestone (Watkinson and Brimacombe, 1982), production of cement (Spang, 1972), alumina (Riffaud et al., 1972), soda ash (Kim and Srivastave, 1991), titanium dioxide (Dumont and Belanger, 1978), catalysts (Groen et al., 1986), waste incineration (Tillman et al., 1990) and fine powders of novel ceramics such as titanium diboride (Shaffer, 1986), solid oxide fuel-cells (Balachandran et al., 1992) or high temperature superconductors (Balachandran et al., 1992; Shelukar et al., 1994).

The objective of this article is to check which physical processes have the main impact on the axial dispersion in a continuous rotary kiln reactor operating at a uniform bed depth. Several stochastic algorithms accounting for different physical processes are used to generate single particle trajectories in the kiln. The simulations check the impact of rolling time, finite thickness of the rolling layer, and the segregated rolling or slumping distance on the dispersion in rolling or slumping beds. Comparing the predictions of the various algorithms enables us to determine the rate processes which need to be accounted for in a model that can predict the experimentally measured Peclet numbers ($Pe \approx 10$–10^3).

Henein et al. (1983) classified various forms of solid motion through a rotating kiln as slipping, slumping, rolling, cascading, cataracting, and centrifuging beds. Only the first three motions (Figure 1) occur in kilns used for calcination, which operate at relatively low rotation rates. In a slipping bed, the solid particles slide against the kiln wall and the bed acts as a rigid solid body with little axial and transverse mixing. The solid is carried along the wall up to the static bed-to-wall angle of repose, then slides down against the wall until reaching the dynamic bed-to-wall repose angle and the process repeats itself. In a slumping bed, the solid particles are carried upwards along the kiln wall up to the bed-to-bed static angle of repose, then slump downward by periodic "avalanches" as a segment of the bed detaches itself from the top of the bed.

Correspondence concerning this article should be addressed to D. Luss.

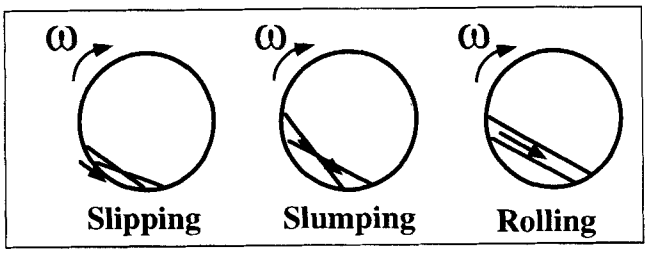

Figure 1. Motions in rotary kilns used for calcination.

At the end of each slump, the inclination angle of the solid with the kiln wall is the dynamic bed-to-bed repose angle. In this motion both axial and transverse mixing occurs. In a rolling bed, the solids flow as a continuous layer on top of the bed. The inclination angle with the kiln wall is the dynamic bed-to-bed repose angle. The rolling layer is continuously fed with solid from the bulk due to the kiln rotation. Both axial and transverse mixing occur. Since the axial dispersion is negligible in slipping beds, this work determines axial dispersion only for slumping and rolling flows.

Experimental studies of the average residence time in rotating drums (Sullivan et al., 1927; Bayard, 1945; Varentsov and Yufa, 1961; Zablotny, 1965; Chatterjee et al., 1983a,b; Perron and Bui, 1990) yield empirical correlations, valid only for specific materials and operating conditions. Room temperature measurements of the residence time distribution (RTD) in rotating drums were done by tracer techniques, such as counting and weighing of dyed particles (Rutgers, 1965b; Abouzeid et al., 1974; Karra and Fuerstenau, 1977; Sai et al., 1990), or using atomic absorption spectroscopy to measure tracer concentration (Wes et al., 1976; Arlyuk and Shakhov, 1982). High temperature RTD measurements were done using radioactive tracers (Costa and Peterman, 1959; Groen et al., 1986). The measured range of the *Pe* numbers varies from 10–100 for short mixing drums (Abouzeid et al., 1974; Wes et al., 1976), to 10^3 for calcination kilns (Groen et al., 1986; Sai et al., 1990).

Figure 2 is a schematic of rotary kiln. We denote by α the kiln inclination angle, θ the solid repose angle, ϕ the angle by which the solids advance axially, φ the solid fill angle, F_s the solid mass-flow rate, L the kiln length, R the kiln radius, and ω the kiln rotation rate.

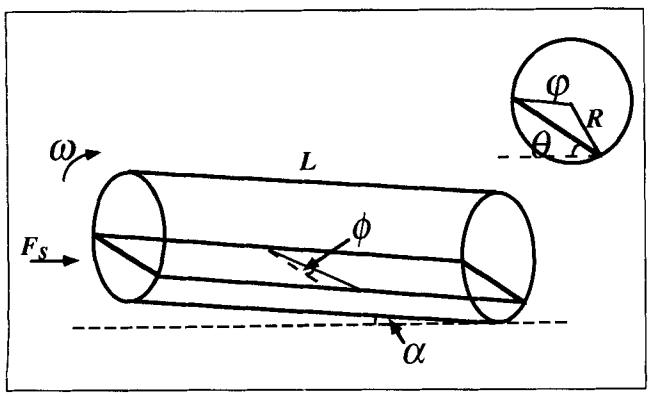

Figure 2. Continuous rotary kiln reactor.

Saeman (1951) developed a model predicting the average residence time of the solid particles in deep and shallow rolling beds. It predicts adequately the average residence time of rolling beds in CRKs (Saeman, 1951; Tscheng and Watkinson, 1979; Groen et al., 1986). For heavily loaded kilns, Saeman predicted that:

$$\tau = \frac{3L \sin \theta_{d-bb}(\varphi - \sin \varphi)}{8\pi R \omega \tan \alpha \sin^3(0.5\varphi)} \tag{1}$$

where θ_{d-bb} is the dynamic bed-to-bed repose angle and φ is the solid fill angle which depends on the percent fill or mass-flow rate. Increasing the solid fill level from 1% to 25% increases the average residence time by 30%. For lightly loaded kilns, the filling angle for each radius of particle path φ_r is small so that $\sin(0.5\varphi_r) \cong 0.5\varphi_r$ and the radius of the different paths is essentially the kiln radius. In such cases Eq. 1 becomes:

$$\tau = \frac{L \sin \theta_{d-bb}}{2\pi R \omega \tan \alpha} \tag{2}$$

Thus, in shallow beds, the average residence time does not explicitly depend on the solid particles fill level or their mass-flow rate.

Previous models described the flow in the kiln by a network of ideal flow systems, the parameters of which are adjusted to fit the experimental RTD data. Fan and Ahn (1961), Rutgers (1965a), Abouzeid et al. (1974), Wes and Drinkenburg (1976), Karra and Fuersenau (1977), Hehl et al. (1978) and Sai et al. (1990) proposed the use of an axial dispersion model with an appropriate *Pe* number determined by experiments. Rutgers (1965a), Groen et al. (1986) and Sai et al. (1990) used the n tanks-in-series model to fit experimental RTD curves. These models do not describe the actual solid flow in the system. Mu and Perlmutter (1980) developed an axial dispersion model, which takes into account some of the key flow features of the solids. It simulates the flow by N rolling steps, each consisting of a flow through a tube followed by a well mixed vessel with bypass and recycle. The model contains three parameters, one of which has to be obtained from RTD experiments.

Rogers and Gardner (1979) extended Saeman's model and used a Monte Carlo simulation to predict the axial dispersion for powder flow in horizontal rotating drums with variable bed depth. They followed the movement of many particles and calculated the axial displacement as well as the time elapsed in each rolling step. The radius of path for each particle movement cycle was determined by a uniform random distribution, while the angle of descent along the cylinder was determined by a normalized Gaussian distribution, the standard deviation of which was adjusted to fit the experimental axial dispersion coefficient.

We use here several stochastic algorithms to determine which physical phenomena have the main impact on the axial dispersion in rolling and slumping beds. The trajectories of individual particles are used to compute the moments of the residence time density function and to determine the axial Peclet number. Knowing the magnitude of the axial dispersion is important for predicting the extent it affects the prod-

uct quality in a calcination process. This can be especially important in multireaction calcination processes in which excessive residence time may cause product decomposition.

Stochastic Simulations of Particle Motion in the Kiln

Development of mathematical model

Rolling Bed. The axial displacement of a particle in a single rolling step is (Saeman, 1951):

$$\Delta z = \Delta l \frac{\tan \alpha}{\sin \theta_{d-bb}} \tag{3}$$

where Δl is the distance the particle rolls on the surface of the bed. The time of rise in a single rolling step is:

$$t_{up} = \frac{\varphi_r}{2\pi\omega} \tag{4}$$

where φ_r is the filling angle corresponding to radius r, the distance from the center of the kiln to the final position of the particle after its roll. The above equations describe the basic rolling or slumping motion. For rolling beds, they are valid if the rolling layer is very thin and the roll time is much smaller than the rise time. In the first random model, denoted as model 1, Eqs. 3 and 4 are used to follow a single particle which, starting from an initial random point, rolls down to a random point, rises with the rotating bed to the symmetric position, and then falls down to a new random point. The numerical algorithm consists of an initialization step which selects a random location, x_1, y_1, on chord DO (Figure 3a). Then a random location x_2, y_2 is selected on chord OD′ and the axial displacement Δz is calculated by Eq. 3 where Δl is the distance of particle roll on the chord DD′. A new symmetric location on chord DO is calculated as well as the time of rise from x_2, y_2 to the symmetrical location using Eq. 4 where $\varphi_r = 2\cos^{-1}(h/\sqrt{x_2^2 + y_2^2})$ and h is the shortest distance from the kiln axis to the bed surface. A new random location x_2, y_2 is then selected and the procedure is repeated until the particle exits the kiln. A detailed description of the calculation of x_1, y, x_2 and y_2 in all the models is given in the Appendix.

Due to the kiln circular cross section, more particles roll from regions close to the wall. The probability of selecting a random number uniformly inside a circle is inversely proportional to its area, that is, inversely proportional to the radius squared. Therefore, in order to sample uniformly the line of solids roll (chords DO or OD′), we multiply the length of the chord by the square root of a uniform random number between zero and one. A FORTRAN-77 uniform random number generator was used in the simulations. Two other generators recommended by Press et al. (1989) were used to check it. All three were found to be adequate using the Chi-Square technique (Knuth, 1981). The random number generators recommended by Press et al. (1989) required longer computation time and hence were not used.

Several models which account for additional processes affecting the particle motion were developed to assess their impact on the dispersion in the kiln. Model 2 accounts for the

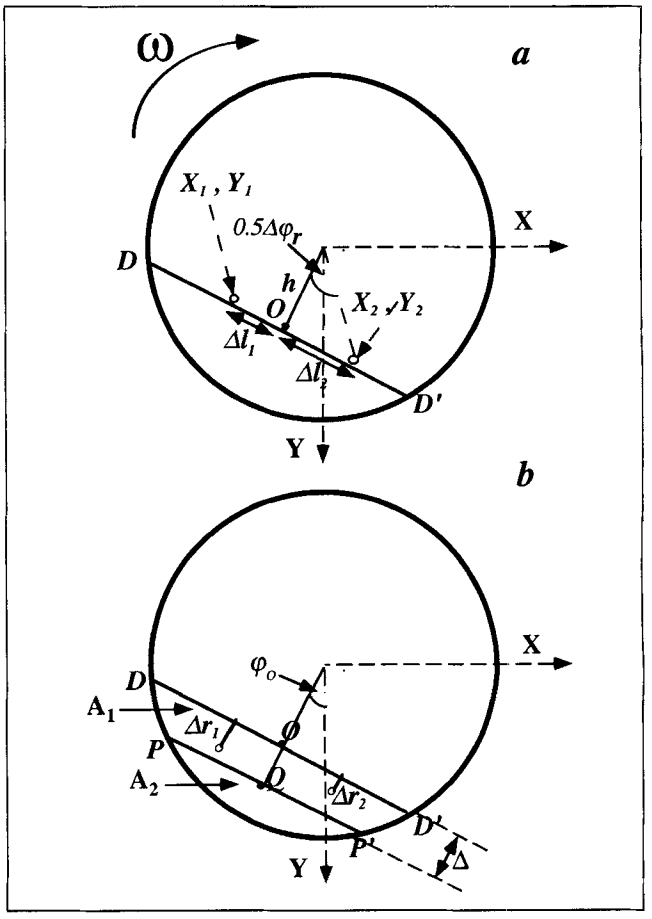

Figure 3. Rolling bed with a thin (a) and thick (b) rolling layer.

time of roll in addition to the time of rise. The distance of roll over an angle of φ_r on chord DOD′ (Figure 3a) is $0.5g \sin \theta_{d-bb} t^2$, which also equals to $2r \sin(\varphi_r/2)/\cos \phi$. Thus, the time of roll neglecting the friction and centrifugal forces is:

$$t_{\text{down}} = 2\sqrt{\frac{r \sin(0.5\varphi_r)}{g \sin \theta_{d-bb} \cos \phi}} \tag{5}$$

where $\phi = \tan^{-1}(\tan \alpha / \sin \theta_{d-bb})$.

This algorithm follows the same steps as model 1. It computes the time per rolling cycle as the sum of the time of sliding from x_1, y_1 to x_2, y_2, (Eq. 5), and rise from x_2, y_2 to the symmetrical location (Eq. 4).

Model 3, which is an extension of model 2, accounts also for the finite thickness Δ of the rolling layer (Figure 3b). Estimated from geometrical considerations and a mass balance, the cross-sectional area of the rolling layer A_1 (Mu and Perlmutter, 1980) is:

$$A_1 = \frac{R^2}{2}(\varphi - \sin \varphi) - A_2 \tag{6}$$

The cross-sectional area of the stationary layer A_2 is:

$$A_2 = R^2\left(\cos^{-1}\left(\frac{\Delta}{R}+\cos\frac{\varphi}{2}\right) - \left(\frac{\Delta}{R}+\cos\frac{\varphi}{2}\right)\sqrt{1-\left(\frac{\Delta}{R}+\cos\frac{\varphi}{2}\right)^2}\right) \quad (7)$$

A mass balance on the rolling and stationary solids gives the relation:

$$A_2\omega = V_{av}\Delta \quad (8)$$

where V_{av} is the average velocity of the rolling particles on top of the solid surface. Accounting only for the gravity force and using Eq. 5, the roll velocity is:

$$V_{\text{down}} = 2\sqrt{\frac{rg\sin(0.5\varphi_r)\sin\theta_{d-bb}}{\cos\phi}} \quad (9)$$

Averaging it for all possible values of r (h to R), while accounting for the circular geometry, gives:

$$V_{av} = \frac{8}{5}\sqrt{\frac{Rg\sin(0.5\varphi)\sin\theta_{d-bb}}{\cos\phi}} \quad (10)$$

The above derivation ignores the impact of friction on the time of roll and thus underestimates the thickness of the rolling layer.

The algorithm initialization step selects a uniform random location x_1, y_1 in DOQP (Figure 3b). Then a random location x_2, y_2 is selected in D'OQP' and the corresponding axial displacement Δz is calculated by Eq. 3 where Δl is the distance of particle rolls in DD'P'P and θ is replaced by $\theta_r = \tan^{-1}((y_2 - y_1)/(x_2 - x_1))$. The new symmetric x_1, y_1 location in DOQP is calculated as well as the time of roll from x_1, y_1 to x_2, y_2 and the time of rise from x_2, y_2 to the symmetrical location (Eqs. 5 and 4). The procedure is repeated until the particle exits the kiln.

Model 4 is an extension of model 3, which accounts for segregated rolling distances. The previous models considered the rolling distance to be random. This represents a bed in which the particles flow properties are uniform. In reality, variation in particle size, density and shape always exists. These variations in the physical and flow properties of the particles enhance radial segregation in rotary kilns. Solid particles segregation due to nonuniform physical properties is mainly due to segregation by flow (Herein et al., 1985). This occurs when large, heavy or round particles tend to roll longer distances than small, light or irregular particles, which tend to be stopped as they roll downwards. Particle-size segregation has been investigated by Herein et al. (1985) and Nityanad et al. (1986) who showed that the small particles tend to accumulate at the center of the bed. The extent and impact of segregation may be very significant when the variation in the particle flow properties is large, for example, when the calcination leads to particle agglomeration (Shelukar et al., 1994). Density segregation may occur when the feed consists of several types of solid particles, such as in direct reduction processes (Venkateswaran and Brimacombe, 1977). Thus, when the bed consists of nonuniform particles, the roll distance of any particle depends on its size, density and shape and is not a random distance, as assumed in models 1–3.

Due to segregation, the roll distance of a particle is dispersed around a point $\bar{X}$. The variance σ of this distance decreases with an increase in the segregation level in the bed. Due to the lack of a predictive model about the relation between the segregated roll distance and the variation in particle physical properties, we assumed that $\bar{X}$ is symmetric to the particle start of roll position. Thus, in our model different particles start of roll positions correspond to particles with different flow properties. For example, small particles are represented by particles with small $\bar{X}$, while large ones are represented by those with large $\bar{X}$. We assume that the dispersion of rolling distances may be described by a truncated Gaussian distribution (Lapin, 1983), with an average $\bar{X}$, and a standard deviation σ. We selected a Gaussian distribution, since the central limit theorem predicts that when a physical phenomenon is the cumulation of many random effects, it tends to be defined by a normal distribution irrespective of the distribution of individual effects (Soong, 1981). The standard deviation of the Gaussian distribution is normalized with respect to l_s, the half length of the rolling layer surface, that is:

$$\sigma = al_s \quad (11)$$

After each roll, the particle moves to a point symmetric to its end of roll position. The numerical algorithm follows the same steps as model 3 with the modification that x_2, y_2 is chosen by a truncated Gaussian distribution.

Slumping Bed. The difference between the static and dynamic bed-to-bed angles of repose determines the slumping volume. When this difference is small, the bed flow is similar to that in a rolling bed. Hence, replacing θ_{d-bb} in Eqs. 1 and 3 with the average $(\theta_{s-bb} + \theta_{d-bb})/2$ where θ_{s-bb} is the static bed-to-bed repose angle, gives an approximate value of τ in a slumping bed.

Model 5 describes the basic flow in a slumping bed using Eqs. 3 and 4 to follow the motion of a single particle. It is similar to rolling model 1, but instead of a continuous roll, it accounts for periodic slumping from the upper to the lower volume. A slump occurs when the bed surface reaches the static bed-to-bed repose angle. Thus, a particle rising along the kiln wall may slump down as soon as it reaches the slumping volume, even before reaching a position symmetrical to that before the start of the rise. On the other hand, the particle may rise above the symmetrical point, as long as the bed surface inclination is smaller than the static bed-to-bed repose angle. The first step in model 5 selects a random location x_1, y_1 in DOS (Figure 4). Next, a random location x_2, y_2 is selected in S'OD' and the axial displacement Δz is calculated by the relation:

$$\Delta z = \tan\alpha\left(\frac{\Delta l_1}{\sin\theta_{r1}} + \frac{\Delta l_2}{\sin\theta_{r2}}\right) \quad (12)$$

where Δl_1, θ_{r1}, and Δl_2, θ_{r2} are the distance and the inclination angle of the slumping particle in the upper and lower

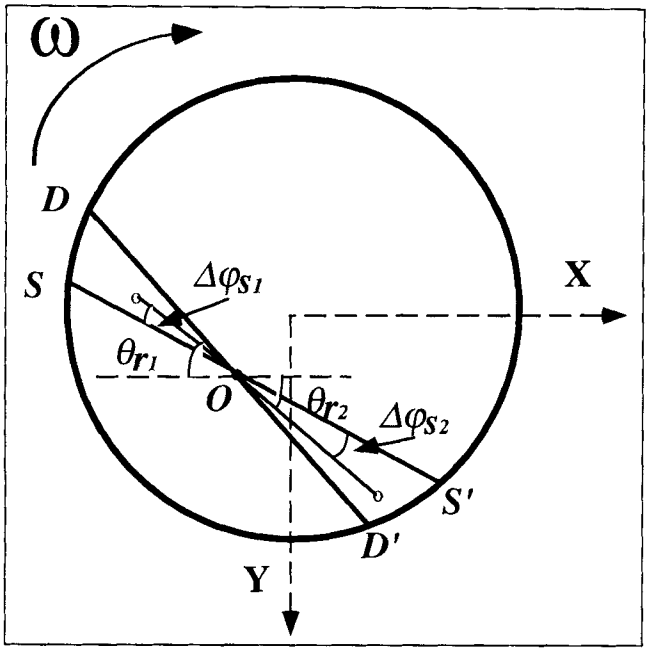

Figure 4. Slumping bed.

slumping volumes, respectively (Figure 4). A new x_1, y_1 location in DOS is selected. The time of rise from x_2, y_2, to the new location in DOS depends on the final rising location.

The particle rises within the slumping volume until slumping occurs. The algorithm assumes that the final point of rise (x_1, y_1) is at a random location on an arc within DOS, the distance of which from point 0 is equal to that between 0 and the start of rise point (x_2, y_2). The corresponding time of rise is computed by Eq. 4. We continue to follow the particle motion until it leaves the kiln. The impact of segregated slumping distance due to dispersion in flow properties is accounted for in model 6. This model follows the same steps as model 5 with the exception that x_2, y_2 in S'OD' is chosen using a truncated Gaussian distribution.

Moments calculation and Peclet number determination

The first three moments of the solids residence time in the kiln define the average, standard deviation and the skewness of the residence time density function (Press et al., 1989). The average residence time is computed by the relation:

$$\tau = \frac{1}{N}\sum_{i=1}^{N} t_i \tag{13}$$

where N is the number of particles and t_i is the residence time of particle i.

The variance is defined as:

$$\sigma^2 = \frac{1}{N-1}\sum_{i=1}^{N} (t_i - \tau)^2 \tag{14}$$

The relative variance satisfies the relation:

$$\sigma_r^2 = \frac{\sigma^2}{\tau^2} \tag{15}$$

The skewness:

$$S = \frac{1}{N}\sum_{i=1}^{N}\left(\frac{t_i - \tau}{\sigma}\right)^3 \tag{16}$$

characterizes the asymmetry of a distribution around its mean. Positive skewness implies a longer "tail" beyond the mode. The trajectories of 2,500 particles were followed in the calculation of τ and σ and 15,000 in the calculation of S. The expected error of these simulations is $\pm 1\%$ for the average residence time and $\pm 4\%$ for the axial dispersion σ_r^2. In general, more trajectories need to be computed for adequate calculation of the higher moments.

In most cases, the dispersion is adequately described by the axial dispersion model (Levenspiel and Smith, 1954), that is,

$$f(\hat{t}) = \frac{1}{\sqrt{4\pi\hat{t}/Pe}}\exp\left(-\frac{(\hat{t}-1)^2}{4\hat{t}/Pe}\right) \tag{17}$$

where Pe, the ratio of convection to diffusion times, is defined as $V_s L/D_a$, V_s being the average solids axial velocity and D_a the axial dispersion coefficient; $\hat{t}$ is a dimensionless time tV_s/L. Levenspiel and Smith (1954) show that for large Pe values ($Pe > 100$):

$$Pe = \frac{V_s L}{D_a} = \frac{2}{\sigma_r^2} \tag{18}$$

When the residence time density function is positively skewed and nonsymmetric, the axial dispersion model is not valid. In such cases we characterize the axial dispersion by σ_r^2, the relative variance.

Results and Discussion

Numerical simulations were carried out to determine the impact of the phenomena incorporated in the different models and the impact of operating parameters (kiln inclination, kiln rotation rate, solids loading) and kiln configuration (L/D), on the extent of the axial dispersion. In all simulations, unless otherwise stated, we set $L/D = 10$, $\alpha = 5°$, $Fr = 7\times10^{-4}$ rpm and $\theta_{d-bb} = 45°$, for rolling beds and $(\theta_{s-bb} + \theta_{d-bb})/2 = 45°$, $\theta_{s-bb} - \theta_{d-bb} = \Delta\varphi_s = 10°$ for slumping beds.

Rolling bed

The impact of the various solid flow rate processes in the rolling bed models 1–4 on the average residence time and the Peclet numbers is shown in Figures 5a and 5b, respectively. Model 1 is the basic rolling model while model 2 accounts also for the solids rolling time, model 3 includes the effect of the rolling layer thickness, and model 4 accounts for the segregated rolling distances.

The average residence time predicted by the basic rolling bed model 1 is close to the predictions of Eq. 1 developed by

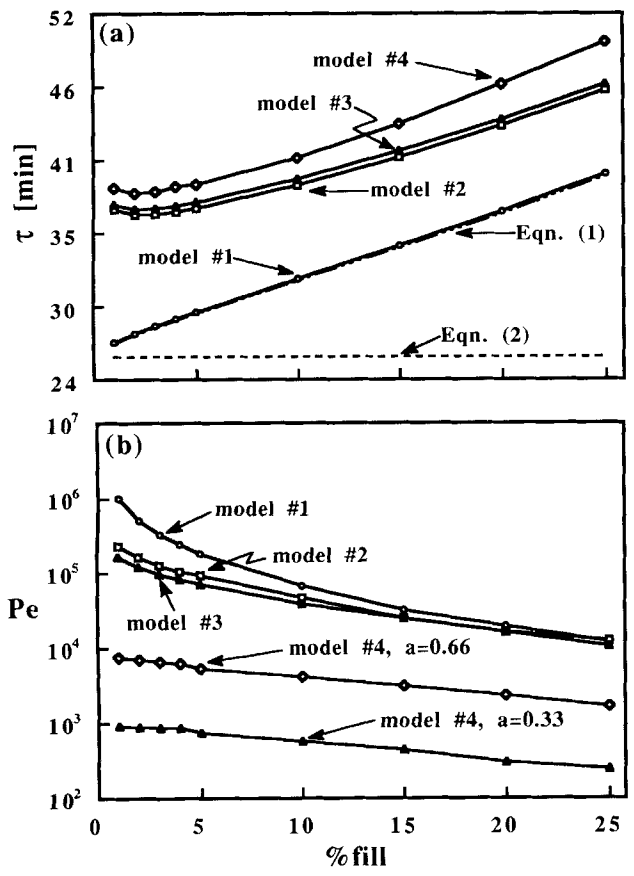

Figure 5. Average residence time compared to Saeman's model (a) and the *Pe* numbers (b) for $Fr = 7 \times 10^{-4}$, obtained from models 1–4 for rolling beds.

Saeman (1951) for heavily loaded kilns. However, the average residence time obtained by models 2, 3 and 4 are higher by 20% to 40%, in the range of 1% to 25% fill (Figure 5a). This difference is mainly due to the impact of the solids rolling time. A further increase, by 5% to 10%, is caused by the flow segregation of nonuniform particles. Equation 2, developed by Saeman for lightly loaded kilns, predicts too short residence times, indicating that it is not suitable for most applications. Increasing the solids fill level increases the average residence time since the rising time is increased.

The *Pe* numbers predicted by models 1–3 (Figure 5b), are extremely large (larger than 10^4). This implies that the flow features accounted for in these models do not create significant axial dispersion as each particle follows all the possible rolling distances with the same probability; so that because of the large number of rolling steps, each particle stays about the same time in the kiln. Thus, all particles exit the kiln with negligible dispersion around the average residence time. The roll time and the finite thickness of the rolling layer slightly increase the dispersion (decrease the *Pe* numbers by less than one order of magnitude). It would be difficult to conduct experiments which measure accurately such low level of dispersion or equivalently high Peclet numbers.

Segregation of rolling distances accounted for in model 4 can decrease the Peclet numbers by one to three orders of magnitude. Large segregation of rolling distances, represented by low values of the parameter a defined by Eq. 11, decreases significantly the *Pe* numbers ($10^2 - 10^3$) that is, increases the axial dispersion to a level consistent with that observed experimentally (Groen et al., 1986; Sai et al., 1990). Increasing the solids fill level increases the axial dispersion. The reason is that as the solids fill level increases, the particles rise to higher positions and undergo larger axial displacements in each rolling step, decreasing the number of steps which in turn increases the dispersion.

The dependence of the *Pe* numbers computed by models 1–3 on the kiln configuration (L/D), inclination angle, and the *Fr* numbers at different solid loading was studied by performing simulations in the range of 1–25% solid fill, $L/D = 1.10$, $\alpha = 3° - 7°$, and $Fr = 10^{-7} - 10^{-3}$. A tenfold decrease in the kiln L/D ratio (Figure 6) decreases the *Pe* numbers by two orders of magnitude, the difference decreasing with increasing percent fill. Similarly, increasing the kiln inclination angle increases the axial dispersion, that is, reduces the *Pe* numbers. This effect is less significant than the effect of the kiln L/D ratio. Increasing the kiln inclination from $3° - 7°$ reduces the *Pe* numbers by a half of an order of magnitude.

While gravitation affects the rolling time, the centrifugal force affects the rising time. Thus, the dispersion predicted by models 2 and 3 is expected to depend on the Froude number, the ratio of the centrifugal to the gravitational force, in contrast to the predictions of model 1. The influence of the Froude number and the solids fill level on the average residence time, and the *Pe* numbers according to model 3 were checked for 1–25% fill levels and $Fr = 7 \times 10^{-6} - 7 \times 10^{-3}$. The *Pe* numbers predicted by the model are of the order of magnitude of (10^4) and slightly decrease (by less than one order of magnitude) as the Froude number increases from 7×10^{-6} to 7×10^{-3}. These values exceed the experimental finding of Peclet numbers of the order of 10^3 obtained by Groen et al. (1986) and Sai et al. (1990).

For *Fr* numbers exceeding (7×10^{-5}), the time of roll increases the average residence time by 20% to 120% (Figure 7). Thus, the rolling time cannot be neglected as assumed by the first model. The cumulative average time that each parti-

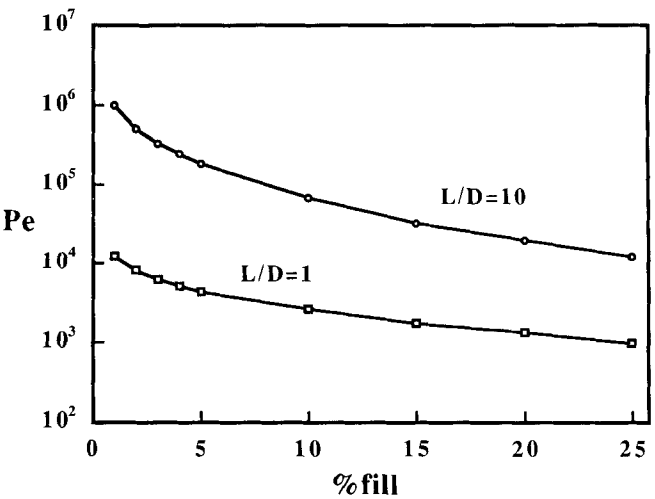

Figure 6. Effect of *L/D* on the *Pe* numbers obtained from model 1.

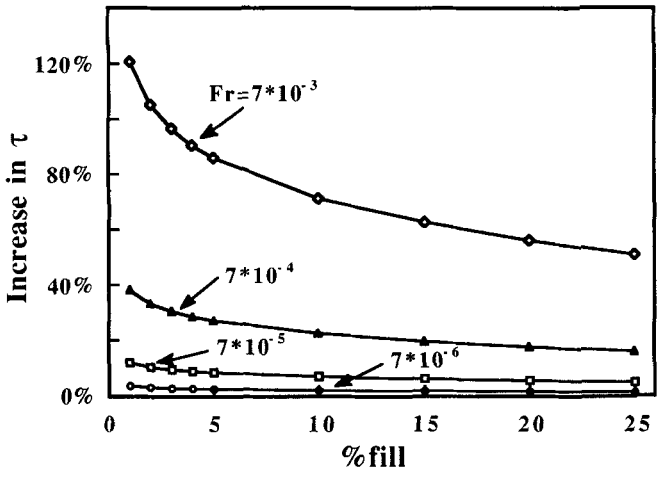

Figure 7. Effect of the *Fr* number on the percentage increase in the average residence time obtained from model 2 compared to that of model 1.

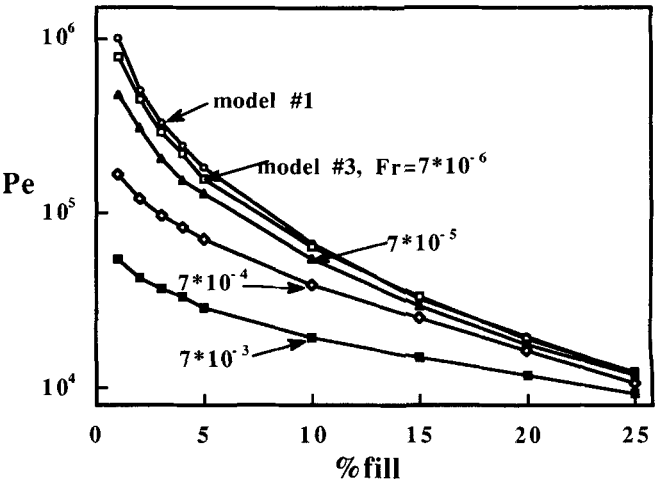

Figure 8. *Pe* numbers obtained from model 3 at various *Fr* numbers compared to the results of model 1.

cle spends rolling on the surface of the solid bed may be expressed as the average time of a single roll multiplied by the average number of rolls. The average number of rolls is the number of kiln rotations $\tau\omega$ multiplied by $2\pi/\varphi$. The average time of a single roll is obtained by averaging Eq. 5 for all possible values of r (h to R), while accounting for the circular geometry. Thus, the ratio of the cumulative average time of roll to the average residence time predicted by Eq. 1 is:

$$\frac{\tau_{\text{roll}}}{\tau} = \frac{16\pi}{5}\frac{\omega}{\varphi}\sqrt{\frac{R\sin 0.5\varphi}{g\sin\theta_{d-bb}\cos\varphi}} \tag{19}$$

The cross-sectional area occupied by the rolling and the bulk layers was calculated from Eqs. 6–10 for the range of $Fr = 7\times10^{-6} - 7\times10^{-3}$ and solids fill level of 1%–25%. The fraction of the cross-sectional area occupied by the rolling layer is less than 1% for *Fr* numbers smaller than (7×10^{-5}) and between 1% to 10% for *Fr* numbers between $(7\times10^{-4} - 7\times10^{-3})$. The effect of the rolling layer thickness on the average residence time (Figure 5a) is small (< 5%). Increasing the *Fr* numbers from 7×10^{-6} to 7×10^{-3} decreases the *Pe* numbers by more than one order of magnitude at low percentage fill (< 5%) (Figure 8). As the percentage fill is increased, the impact of the *Fr* number decreases and at 25% it does not affect the *Pe* values. In reality, the thickness of the rolling layer is larger than that predicted by this model because friction slows down the solid motion, so that the thickness of the rolling layer increases. Simulations of model 3 showed that a sixfold increase of the rolling layer thickness, predicted for the frictionless case (Eqs. 7–10), decreases the Peclet numbers by about 30%. These Peclet numbers were of the order of 10^4.

The effect of segregated rolling distance due to dispersion in particle flow properties was studied by simulations of model 4 for distributions with different σ values, that is, different values of a, corresponding to a Gaussian spread of the roll distances around the symmetrical start of roll point at x_1, y_1. As the value of the parameter a is reduced (increased segregation, that is, decreased dispersion in the roll distance), the mode of the residence time density function shifts to lower times and a "tail" develops (Figure 9a), while the axial dispersion increases. For a in the range of 0.66 to 0.167, the relative variance increases by one to three orders of magnitude compared to model 3. The calculated skewness in Figure 9b is $S = 0.68$ and 1.24 for $a = 0.66$ and 0.33 respectively. In such cases the axial dispersion model is no longer a valid representation of the dispersion. Therefore, the relative variance is used to characterize the dispersion instead. The *Pe* numbers reported for model 4 are presented only for comparison to the previous models. The predicted shape of the RTD curves is similar to the experimental results of Costa and Peterman (1959) and Arlyuk and Shakhov (1982).

The trajectory of each particle in model 4 strongly depends on its start of roll location in the bed. The axial displacement of a particle with a large $\bar{X}$ are large on the average and it exits the kiln rapidly and vice versa. Thus, a large dispersion in the number of rolling steps of different particles is obtained. The increased axial dispersion predicted by this model is due to the large variation in the number of rolling steps.

Slumping bed

The average residence time obtained by the basic slumping bed model 5 is very close to the predictions of Eq. 1 developed by Saeman (1951) for rolling beds in heavily loaded kilns. The average residence time obtained by model 6, which accounts for flow segregation is higher by 5% to 10%. The similarity to rolling beds is expected as the slumping volume is symmetric around its center so that an equal number of particles slump with inclination angles steeper or milder than $(\theta_{s-bb} + \theta_{d-bb})/2 = 45°$.

The *Pe* numbers obtained from models 5 and 6 for slumping beds are compared in Figure 10 to those predicted by model 1 for rolling beds. The Peclet numbers predicted by the basic slumping bed model 5 are extremely high (10^4), but lower than the corresponding values (under the same operating and kiln configuration) in rolling beds. While the *Pe*

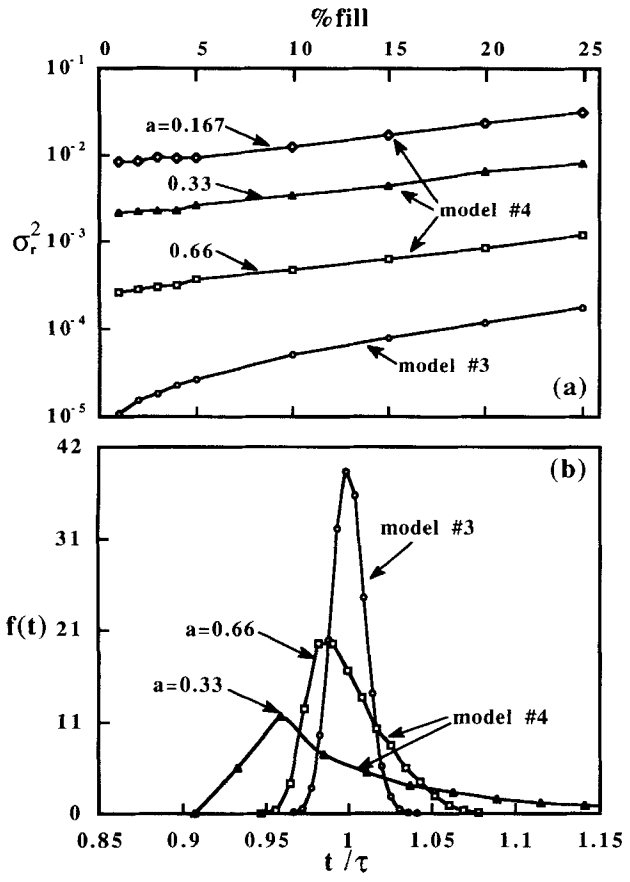

Figure 9. Relative variance (a) and the residence time density functions at 10% fill (b), obtained from model 4 at different values of *a* for $Fr = 7 \times 10^{-4}$, compared to the results of model 3.

numbers in rolling beds decrease monotonically with increasing the solids fill level, they are almost independent of the solids fill level in slumping beds. Thus, at low percentage fill (< 10%), the *Pe* numbers in slumping beds are lower by one to two orders of magnitude from those in rolling beds. The difference decreases with increased percentage fill, until at 25% fill the values are very close. A significant increase in the dispersion is caused by slumping distance segregation, accounted for in model 6. The segregation decreases the *Pe* numbers by two orders of magnitude over the entire range of 1% to 25% fill. Large segregation of slumping distances represented by low values of the parameter a ($a = 0.33$) results in low *Pe* numbers ($10^2 - 10^3$), which are of the order measured by Groen et al. (1986) and Sai et al. (1990).

The slumping volume represented by $\Delta\varphi_s$, the difference between the static and the dynamic repose angle affects the axial dispersion, as shown in Figure 11. The Peclet numbers are close to those for a rolling bed for small $\Delta\varphi_s$. As $\Delta\varphi_s$ increases, the *Pe* numbers decrease monotonically with increasing percentage fill for $\Delta\varphi_s < 2$. However, for large $\Delta\varphi_s$, the Peclet numbers are almost independent of the percentage fill having a broad local maximum. The reason for the low *Pe* values at low percent fill is that the fraction of the slumping volume is large, causing large axial displacements in

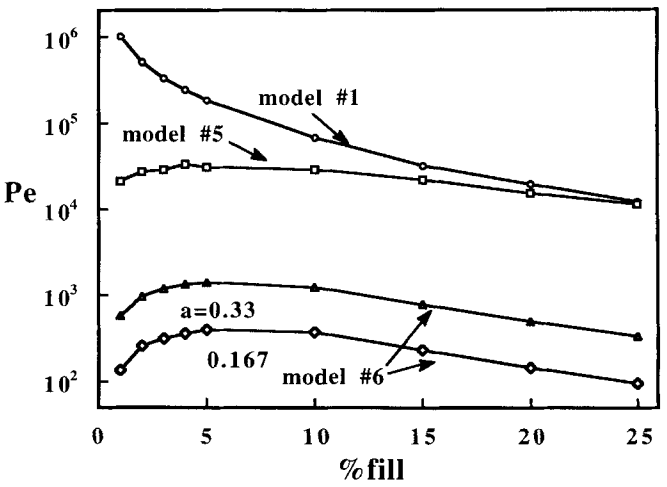

Figure 10. *Pe* numbers obtained from models 5 and 6 for slumping beds with $\Delta\varphi_s = 10°$, compared to the results of model 1 for rolling beds.

each slumping step. As the slumping volume increases, the axial dispersion increases due to the increased dispersion of the axial displacement in each slumping step.

The axial dispersion increases as the parameter a is decreased (Figure 12a). The relative variance increases from (10^{-4}) to (10^{-2}) as a is decreased from 0.66 to 0.167. Similar to the behavior in a rolling bed, as the parameter a decreases, the Gaussian shape of the residence time density function (Figure 12b) becomes less symmetric and a "tail" with increased skewness develops. The calculated skewness values in Figure 12b are $S = 0.23$, 0.96, and 1.50 for $a = 0.66$, 0.33, and 0.167, respectively. Residence time density functions (Figure 10b) for the same a values show that the impact of radial segregation in slumping beds is less significant than in rolling beds.

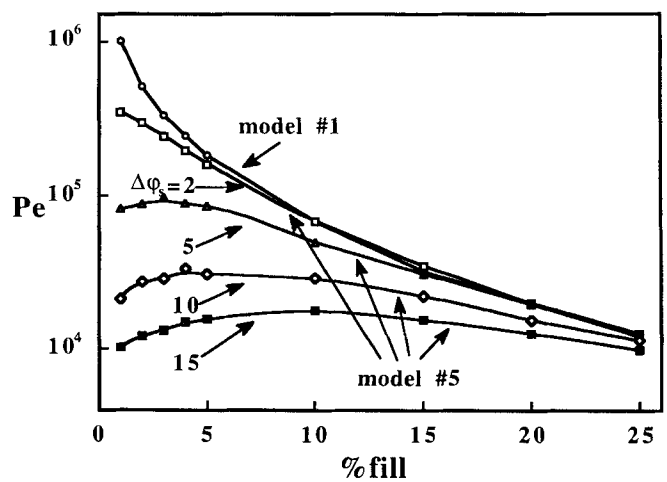

Figure 11. *Pe* numbers obtained from model 5 for slumping beds at different values of $\Delta\varphi_s$, compared to the results of model 1 for rolling beds.

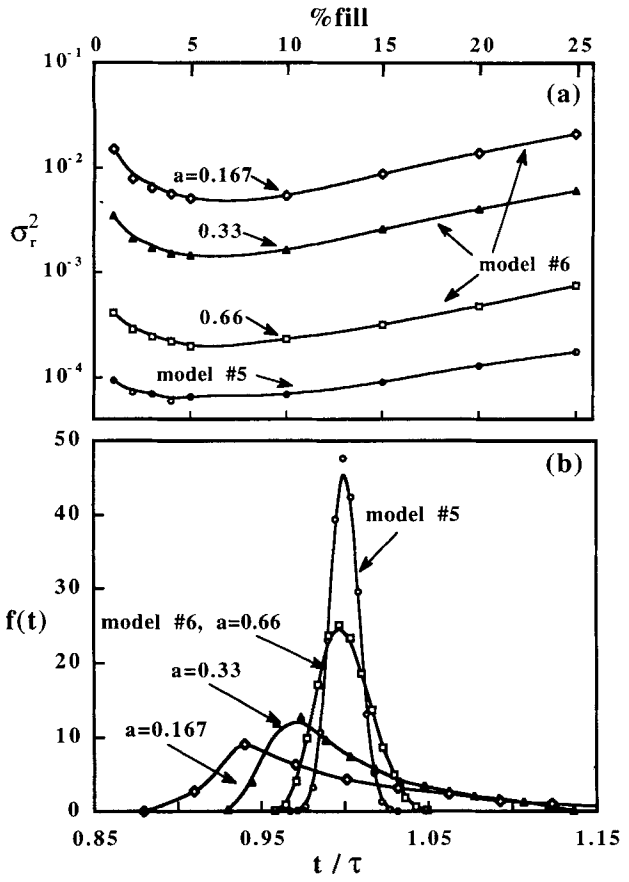

Figure 12. Relative variance (a) and the residence time density functions at 10% fill (b), obtained from model 6 at different values of *a*, compared to the results of model 5.

Concluding Remarks

The simulations demonstrate that while the simple analytical Eq. 1 developed by Saeman (1951) adequately predicts the average solid residence time in CRKs operating at low Froude numbers, additional rate processes need to be considered for prediction of the axial dispersion of the solids in CRK reactors.

The basic rolling and slumping algorithms 1 and 5 predict an average residence time which is very close to that of Eq. 1. For Froude numbers exceeding (7×10^{-5}), the average rolling time predicted by Eq. 19 has to be accounted for (model 2). In most applications of CRK, the correction introduced by this term is small as they rarely operate at $Fr > 7\times10^{-5}$. Simulations indicate that Eq. 1 can predict also the average residence time in slumping beds by replacing θ_{d-bb} with the average $(\theta_{s-bb} + \theta_{d-bb})/2$.

The rolling models 1–3, which describe the basic rolling motion, the rolling time and the finite rolling layer thickness, predict negligible axial dispersion (*Pe* larger than 10^4) for kiln configuration of $L/D = 10$. A monotonic decrease of the *Pe* values is observed as the percentage fill is increased. Decreasing the kiln L/D ratio from 10 to 1 reduces the *Pe* numbers to the order of 10^3. Increasing the Froude numbers from 7×10^{-6} to 7×10^{-3} decreases the *Pe* numbers by more than one order of magnitude at low percentage fill (< 5%). As the percentage fill increases, the impact of the *Fr* numbers decreases and at 25% fill the *Pe* is independent of the values of the *Fr* numbers.

The basic slumping model 5 predicts *Pe* numbers of the order of 10^4 for kiln configuration of $L/D = 10$. The *Pe* values are almost invariant with the solids fill level and a broad local maximum is observed. For large slumping volumes, such as $\Delta\varphi_s = 15°$ and kiln L/D smaller than 10, the *Pe* values are of the order of 10^3. These predicted values in models 3 and 5 exceed experimental results and would be very difficult to determine accurately in an experiment.

The main finding of our simulations is that segregated rolling or slumping distance, considered in models 4 and 6 respectively, significantly increases the axial dispersion, increasing the relative variance to the order of $10^{-3} - 10^{-2}$ and even 10^{-1} (corresponding to *Pe* of order $10^3 - 10^2$ and 10^1) for low *a* values representing highly segregated beds in short kilns with high solids loading. Increased segregation (decreased randomness) in particle rolling or slumping distance increases the spread in the number of rolling or slumping steps among the particles and hence increase the standard deviation of the residence time density function.

The shape of the residence time density function is Gaussian for nonsegregated beds since the solid motion consists of many random events. A positive skewness is introduced by the solid segregation model for which the particle motion is not random. Both Gaussian and positively skewed density functions have been observed experimentally.

High Froude numbers, low L/D ratios, high solids fill levels, large rolling or slumping layer thickness, and, most importantly, flow segregation due to nonuniform particle flow properties increase the axial dispersion and lower the *Pe* numbers.

The simulations show that models which assume random rolling or slumping motion, underestimate the dispersion in the kiln. Models which account for flow segregation predict dispersion values which agree with the magnitude determined in experiments. The main current problem with the use of either model 4 or 6 for a priori prediction of the dispersion is the inability to predict the dependence of the standard deviation of the Gaussian distribution of the roll distance on the properties of the powder. This points out the need to obtain a better understanding and ability to predict the relation between the solids physical and flow properties and the flow segregation in the kiln. An additional complication in predicting the dispersion and its impact occurs when calcination leads to variations in the particles flow properties along the kiln, such as particle agglomeration and sintering during the calcination of superconducting powders (Shelukar et al., 1994).

Acknowledgments

This research was supported by DARPA grant no. MDA 972-88-G-002 and the Texas Center for Superconductivity at the University of Houston. We thank J. D. Schieber and J. Gabitto for helpful discussions about random processes and their application in continuous rotary kilns.

Notation

a = normalized standard deviation defined by Eq. 11
Fr = Froude number, $\omega^2 R/g$

g = acceleration of gravity
h = shortest distance from the kiln axis to the bed surface
l_s = half the length of the rolling layer surface in the kiln cross section
N = number of tracer particles used in the random simulation
P = ratio of the solids rolling layer area to the solids bulk layer area
r = radius of particle path
S = skewness, defined by Eq. 16
t_{down} = rolling time
t_{up} = rising time
V_{roll} = velocity of a single roll
V_s = average solids axial velocity
$\overline{X}$ = start of roll position
z = axial coordinate of the kiln
Δz = axial displacement per one slump or roll

Greek letters

θ_{d-bw} = dynamic bed-to-wall repose angle
θ_{s-bb} = static bed-to-bed repose angle
θ_{s-bw} = static bed-to-wall repose angle
σ = standard deviation, defined by Eq. 14
σ_r^2 = relative variance of the RTD, defined by Eq. 15
τ = average residence time in the kiln, defined by Eq. 13
τ_{roll} = cumulative average rolling time

Literature Cited

Abouzeid, A. S. M. A., T. S. Mika, K. V. Sastry, and D. W. Fuerstenau, "The Influence of Operating Variables on the Residence Time Distribution for Material Transport in a Continuous Rotary Drum," *Powder Tech.*, **10**, 273 (1974).

Arlyuk, B. I., and S. V. Shakhov, "Evaluating the Uniformity of Material Movement in Rotary Kilns," *Sov. Chem. Ind.*, **14**(11), 1383 (1982).

Bayard, R. A., "New Formula Developed for Kiln Time," *Chem. Met. Eng.*, 100 (1945).

Balachandran, U., S. E. Dorris, M. T. Lanagan, R. B. Poeppel, J. M. Tourre, and J. W. Golowski, "Synthesis of Rare-Earth-Based Oxides for the Ceramic Industry: From Laboratory to Pilot Plant," *Mat. Res. Soc. Symp. Proc.*, **249**, 121 (1992).

Chatterjee, A., A. V. Sathe, M. P. Srivastava, and P. K. Mukhopadhyay, "Flow of Materials in Rotary Kilns Used for Sponge Iron Manufacture: 1. Effect of Some Operational Parameters," *Met. Trans. B*, **14B**, 375 (1983a).

Chatterjee, A., A. V. Sathe, and P. K. Mukhopadhyay, "Flow of Materials in Rotary Kilns Used for Sponge Iron Manufacture: 2. Effect Kiln Geometry," *Met. Trans. B*, **14B**, 383 (1983b).

Costa, H., and C. Peterman, "Untersuchungen uber die materialbewegung und staubbildung in drehofen der zement industrie mit hilfe radioaktiver isotope," *Silikatechn.*, **10**(5), 253 (1959).

Dumont, G., and P. R. Belanger, "Steady State Study of Titanium Dioxide in Rotary Kiln," *Ind. Eng. Chem., Proc. Des. Dev.*, **17**(2), 107 (1978).

Fan, L. T., and Y. K. Ahn, "Axial Dispersion of Solids in Rotary Solid Flow System," *Appl. Sci. Res.*, **10A**, 465 (1961).

Groen, G., J. Ferment, M. J. Groeneveld, J. Decleer, and A. Delva, "Scaling Down of the Calcination Process for Industrial Catalyst Manufacturing," *Proc. Int. Symp. Sci. Basis for the Preparation of Heterogeneous Catalysts*, Elsevier, Amsterdam (1986).

Hehl, M., H. Kroger, H. Helmrich, and K. Schugerl, "Longitudal Mixing in Horizontal Rotary Drum Reactors," *Powder Tech.*, **20**, 29 (1978).

Henein, H., J. K. Brimacombe, and A. P. Watkinson, "Experimental Study of Transverse Bed Motion in Rotary Kilns," *Met. Trans. B*, **14B**, 191 (1983).

Henein, H., J. K. Brimacombe, and A. P. Watkinson, "An Experimental Study of Segregation in Rotary Kilns," *Met. Trans. B*, **16B**, 763 (1985).

Karra, V. K., and D. W. Fuerstenau, "Material Transport in a Continuous Rotating Drum. Effect of Discharge Plate Geometry," *Powder. Tech.*, **16**, 23 (1977).

Kim, K. N., and R. Srivastave, "Computer Simulation of an Industrial Calciner with an Improved Control Scheme," *Ind. Chem. Eng. Res.*, **30**, 594 (1991).

Knuth, D. E., "Seminumerical Algorithms," *The Art of Computer Programming*, Vol. 2, 2nd ed., Chap. 3, Reading, MA (1981).

Lapin, L. L., *Probability and Statistics for Modern Engineering*, Chap. 4, Brooks/Cole Eng. Div., Monterey, CA (1983).

Levenspiel, O., and W. K. Smith, "Notes on the Diffusion-Type Model for the Longitudinal Mixing of Fluids in Flow," *Chem. Eng. Sci.*, **6**, 227 (1957).

Mu, J., and D. D. Perlmutter, "The Mixing of Granular Solids in a Rotary Cylinder," *AIChE J.*, **26**(6), 928 (1980).

Mu, J., and R. A. Hard, "Simulation Study of a Phosphate Nodulizing Kiln," *Ind. Eng. Chem., Proc. Des. Dev.*, **23**(2), 374 (1984).

Nityanad, N., B. Manly, and H. Henein, "An Analysis of Radial Segregation for Different Sized Spherical Solids in Rotary Cylinders," *Met. Trans. B*, **17B**, 247 (1986).

Perron, J., and R. T. Bui, "Rotary Cylinders: Solid Transport Prediction by Dimensional and Rheological Analysis," *Can. J. of Chem. Eng.*, **68**, 61 (1990).

Press, W. H., B. P. Flannery, S. A. Teakolsky, and W. T. Vetterling, *Numerical Recipes, The Art of Scientific Computing*, Chaps. 7 and 13, Cambridge Univ. Press, New York (1989).

Riffaud, J. B., B. Koehret, and B. Coupal, "Modeling and Simulation of an Alumina Kiln," *Brit. Chem. Eng. and Proc. Tech.*, **17**(5), 413 (1972).

Rogers, R. S. C., and R. P. Gardner, "A Monte Carlo Method for Simulating Dispersion and Transport through Horizontal Rotating Cylinders," *Powder Tech.*, **23**, 159 (1979).

Rutgers, R., "Longitudinal Mixing of Granular Material Flowing through a Rotating Cylinder. Part 1—Descriptive and Theoretical," *Chem. Eng. Sci.*, **20**, 1079 (1965a).

Rutgers, R., "Longitudinal Mixing of Granular Material Flowing through a Rotating Cylinder. Part 2—Experimental," *Chem. Eng. Sci.*, **20**, 1089 (1965b).

Saeman, W. C., "Passage of Solids through Rotary Kilns," *Chem. Eng. Prog.*, **47**(10), 508 (1951).

Sai, P. S. T., G. D. Surender, A. D. Damodaram, V. Suresh, Z. G. Philip, and K. Sankaran, "Residence Time Distribution and Material Flow Studies in a Rotary Kiln," *Met. Trans. B*, **21B**, 1005 (1990).

Sass, A., "Simulation of the Heat Transfer Phenomena in a Rotary Kiln," *Ind. Eng. Chem., Proc. Des. Dev.*, **6**(4), 532 (1969).

Shaffer, P. T., "Process Study for Manufacturing Ultra Fine Titanium Diboride Powder," *Adv. Res. Tech.*, Rep. No. AD-A170, 136 (1986).

Shelukar, S. D., H. G. K. Sundar, R. Semiat, J. T. Richardson, and D. Luss, "Continuous Rotary Kiln Calcination of YBaCuO Precursor Powders," *I&EC Res.*, **33**, 421 (1994).

Soong, T. T., *Probabilistic Modeling and Analysis in Science and Engineering*, Chap. 7, Wiley, New York (1981).

Spang, H. A., "A Dynamic Model of a Cement Kiln," *Automatica*, **8**, 309 (1972).

Sullivan, J. D., C. G. Maier, and O. C. Ralson, "Passage of Solid Particles through Rotary Cylindrical Kilns," U.S. Bur. of Mines, Tech. paper, No. 384, 1 (1927).

Tillman, D. A., A. J. Rossi, and K. M. Vick, "Rotary Incineration Systems for Solids Hazardous Wastes," *Chem. Eng. Prog.*, **86**, 19 (1990).

Tscheng, S. H., and T. P. Watkinson, "Convective Heat Transfer in a Rotary Kiln," *Can. J. of Chem. Eng.*, **57**, 433 (1979).

Watkinson, A. P., and J. K. Brimacombe, "Limestone Calcination in a Rotary Kiln," *Met. Trans. B*, **13B**, 369 (1982).

Wes, G. W. J., A. A. H. Drinkenburg, and S. Stemerding, "Solid Mixing and Residence Time Distribution in a Horizontal Rotating Drum Reactor," *Powder Tech.*, **13**, 177 (1976).

Varentsov, P. V., and M. S. Yufa, "The Movement of a Bed of Solid Particles in Rotary Kilns," *Int. Chem. Eng.*, **1**(1), 88 (1961).

Venkateswaran, V., and J. K. Brimacombe, "Mathematical Model for SL/RN Direct Reduction Process," *Met. Trans. B*, **8B**, 387 (1977).

Zablotny, W. W., "The Movement of the Charge in Rotary Kilns," *Int. Chem. Eng.*, **5**(2), 360 (1965).

Appendix: Calculation of x_1, y_1 and x_2, y_2 in All Models

Models 1 and 2

The initial x_1, y_1 location (Figure 3a) is calculated by:

$$x_1 = x_o + (x_D - x_o)\frac{\Delta l_1}{l_s} \tag{A1}$$

$$y_1 = y_o + (y_D - y_o)\frac{\Delta l_1}{l_s} \tag{A2}$$

where $l_s = 0.5\sqrt{(x_D - x_{D'})^2 + (y_D - y_{D'})^2}$, $\Delta l_1 = l_s\sqrt{\text{ran}}$ and ran is a random number between 0–1.

The x_2, y_2 location is calculated by:

$$x_2 = x_o - (x_o - x_{D'})\frac{\Delta l_2}{l_s} \tag{A3}$$

$$y_2 = y_o - (y_o - y_{D'})\frac{\Delta l_2}{l_s} \tag{A4}$$

where $\Delta l_2 = l_s\sqrt{\text{ran}}$.

The symmetric x_1, y_1 location is calculated by:

$$x_1 = 2x_o - x_2 \tag{A5}$$

$$y_1 = 2y_o - y_2 \tag{A6}$$

Models 3 and 4

The initial x_1, y_1 location (Figure 3b) is calculated by:

$$x_1 = x_o + (x_D - x_o)\frac{\Delta l_1}{l_s} - \Delta_{r1}\sin\varphi_o \tag{A7}$$

$$y_1 = y_o + (y_D - y_o)\frac{\Delta l_1}{l_s} + \Delta_{r1}\cos\varphi_o \tag{A8}$$

where $\Delta l_1 = l_s\sqrt{\text{ran1}}$, $\Delta_{r1} = \Delta\text{ran2}$, and ran1, ran2 are random numbers between 0–1.

The x_2, y_2 location is calculated by:

$$x_2 = x_o - (x_o - x_{D'})\frac{\Delta l_2}{l_s} - \Delta_{r2}\sin\varphi_o \tag{A9}$$

$$y_2 = y_o - (y_o - y_{D'})\frac{\Delta l_2}{l_s} + \Delta_{r2}\cos\varphi_o \tag{A10}$$

where $\Delta l_2 = l_s\sqrt{\text{ran1}}$ is used in model 3, while $\Delta l_2 = al_s\text{gran} + \Delta l_1$ is used in model 4 with a standard Gaussian random number with zero mean and unit variance, gran, and $\Delta_{r2} = \Delta\text{ran2}$.

The symmetric x_1, y_1 location is calculated by:

$$x_1 = 2(x_o - \Delta_{r2}\sin\varphi_o) - x_2 \tag{A11}$$

$$y_1 = 2(y_o + \Delta_{r2}\cos\varphi_o) - y_2 \tag{A12}$$

Models 5 and 6

The initial x_1, y_1 location (Figure 4) is calculated by:

$$x_1 = x_o - \Delta l_1\cos\theta_{r1} \tag{A13}$$

$$y_1 = y_o - \Delta l_1\sin\theta_{r1} \tag{A14}$$

where $\Delta l_1 = l_o\sqrt{\text{ran1}}$ with l_o the length of line DO, and $\theta_{r1} = \Delta\varphi_{s1} + \theta_{-bb}$ with $\Delta\varphi_{s1} = \Delta\varphi_s\text{ran2}$.

The x_2, y_2 location is calculated by:

$$x_2 = x_o + \Delta l_2\cos\theta_{r2} \tag{A15}$$

$$y_2 = y_o + \Delta l_2\sin\theta_{r2} \tag{A16}$$

where $\Delta l_2 = l_o\sqrt{ran1}$ is used in model 5 while $\Delta l_2 = al_o\text{gran} + \Delta l_1$ is used in model 6, and $\theta_{r2} = \Delta\varphi_{s2} + \theta_{-bb}$ with $\Delta\varphi_{s2} = \Delta\varphi_s\text{ran2}$.

The new x_1, y_1 is located within the slumping volume DOS at a distance Δl_2 from point 0. Its angular position is determined by multiplying $\Delta\varphi_s$ by a random value, ran2.

Manuscript received June 30, 1994, and revision received Dec. 16, 1994.